SIMULTANEOUS INCORPORATION OF Cr, Zn, Cd, AND Pb
IN THE GOETHITE STRUCTURE

Navdeep Kaur[1], Markus Gräfe[1], Balwant Singh[1],*, and Brendan Kennedy[2]

[1] Faculty of Agriculture, Food & Natural Resources, The University of Sydney, NSW 2006, Australia
[2] School of Chemistry, The University of Sydney, NSW 2006, Australia

Abstract—In order to improve our understanding of how the goethite crystal structure is affected by the incorporation of metals (and by variations in the amount of the incorporation), and to review any possible synergistic and antagonistic effects of co-metals, the present investigation focused on the incorporation of multiple (di-, tri-, and tetra-) metals, *i.e.* Cr, Zn, Cd, and Pb, in the goethite crystallographic structure. A series of single- and multi-metal M-Cr/Zn/Cd/Pb-substituted goethites with $M/(M+Fe)$ molar ratios = 0.10 were prepared. The general sequence of metal entry in single-metal substituted goethites was Zn = Cr > Cd > Pb and in multi-metal-substituted goethites was Zn > Cr $\geqslant$ Cd > Pb. Simultaneous incorporation of Cr, Zn, Cd, and Pb up to 10.5 mole % was achieved in goethite. Synchrotron X-ray diffraction and extended X-ray absorption fine structure (EXAFS) techniques were employed to assess the structural characteristics of the synthesis products. Rietveld refinement of XRD data showed small changes in unit-cell parameters and Fe/M−Fe/M distances due to M substitution(s). A typical goethite-like crystalline structure remained intact, however. The unit-cell parameters were mutually, linearly correlated, though Fe/M−Fe/M distances were not, indicating that complex changes occurred at the local scale. In single-metal substituted goethites, incorporation of Cr reduced the unit-cell volume by 0.13% while that of Zn, Cd, and Pb increased it by 1.09, 3.58, and 0.56%, respectively. The changes in multi-metal-substituted goethites appeared to be the complex combination of that of the individually incorporated metals. The X-ray absorption near edge structure study of Pb-substituted goethites showed that the majority of associated Pb was Pb^{2+}, while Pb^{4+} was preferred over Pb^{2+} in the bulk structure. Measurements by EXAFS at the Fe K-edge indicated that the Fe polyhedra contracted in the presence of Cd^{2+} and Pb^{2+}, providing room for the substitution of larger cations. Measurements by EXAFS at the Cr and Cd K-edges indicated symmetric Cr/Cd polyhedra with single Cr/Cd−O distances and, at Fe and Zn K-edges and the Pb L_{III}-edge, indicated asymmetric polyhedra with two sets of Fe/Zn/Pb−O distances. The Zn octahedra were possibly $Zn(OH)_4O_2$, which enlarged the metal–metal corner-sharing distance to 3.86 Å. This configuration of ligands around the Zn^{2+} cation might occur to balance local charges. Symmetric polyhedra appeared to reduce steric strains in the structure, compared to the asymmetric polyhedra. The result was that Cr enhanced the incorporation of Zn, Cd, and Pb, while the converse was true for Zn.

Key Words—Cr, Zn, Cd, Pb, single, multiple, metal substitution, XRD, EXAFS, goethite.

INTRODUCTION

Goethite (α-FeOOH) is the most common Fe oxide in soils and ores (Singh and Gilkes, 1992). It is isostructural with diaspore (α-AlOOH) and other metal oxides (Cornell and Schwertmann, 2003). The double chains of Fe octahedra ($FeO_3(OH)_3$) formed by edge-sharing (E_2) run parallel to the [010] direction (space group *Pnma*) (Figure 1). These chains are linked to adjacent double chains by corner sharing (CS) with one chain being displaced by $b/2$ with respect to its neighbors (Cornell and Schwertmann, 2003). The three Fe−Fe distances in the structure formed from such a linkage are two edge sharing, $E_1 \approx 3.01$ and $E_2 \approx 3.28$ Å and one corner sharing, CS ≈ 3.46 Å (Figure 1) (Manceau and Drits, 1993). This arrangement of the double chains leads to

the orthorhombic symmetry with unit-cell dimensions $a \approx 9.956$, $b \approx 3.021$, and $c \approx 4.608$ Å (Figure 1) (Szytula *et al.*, 1968).

Goethite is well known for its association with a number of cations that are iso- or heterovalent to Fe^{3+} (Singh and Gilkes, 1992; Singh *et al.*, 1997; Manceau *et al.*, 2000; Singh, 2001). In natural environments and in many industrial processes, goethite forms in the presence of multiple metallic cations. To date, however, only three studies have investigated multiple metal substitutions in goethite (Cornell, 1991; Manceau *et al.*, 2000; Alvarez *et al.*, 2007). Cornell (1991) successfully incorporated up to 8 mole % Ni, Co, and Mn into goethite. Alvarez *et al.* (2007) synthesized goethites with different Al:Mn ratios with a maximum substitution of 12 mole %. Manceau *et al.* (2000) observed simultaneous incorporation of Cr (0.73%), Mn (0.88%), Co (0.17%), Ni (0.90%), Cu (0.263%), and Zn (0.026%) in natural goethite.

Cornell (1991) observed that the preferential order for metal to Fe^{3+} substitution in goethite was: Mn^{3+} =

* E-mail address of corresponding author:
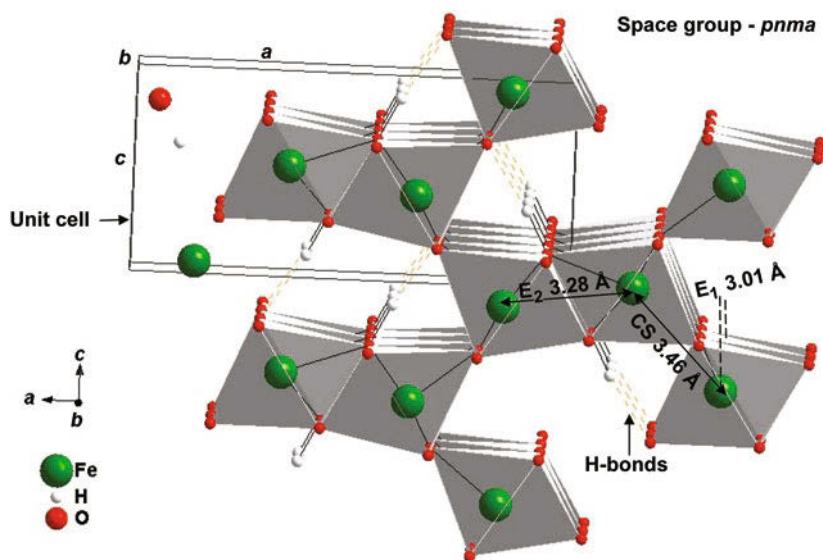b.singh@usyd.edu.au

Figure 1. The structure of goethite showing the three Fe$-$Fe distances, two edge-sharing (E_1 and E_2) and one corner-sharing (CS) (Manceau and Drits, 1993), and the unit cell with its dimensions *a*, *b*, and *c* (Szytula *et al.*, 1968).

$Co^{3+} > Ni^{2+}$, in the di- and tri-metal systems, attributing the small uptake of Ni to its smaller valence state and larger cationic size. Cornell (1991) also observed that the preferential order of metal incorporation in goethite was the reverse of the order of metal re-adsorption on ferrihydrite (Ni $\gg$ Co > Mn), which could be another factor governing the extent of isomorphous substitution in this system. Alvarez *et al.* (2007) observed the dominance of Mn over Al in simultaneous incorporation of these two ions in the goethite structure. The EXAFS measurements showed that Mn^{3+} caused significant structural strain due to its Jahn-Teller behavior, and thereby inhibited incorporation of Al. In contrast, the structural contraction due to the presence of Al restrained the axial distortion of Mn^{3+} and thereby enhanced incorporation of Mn^{3+} in goethite. Those authors observed that the increasing Mn^{3+} substitution, and consequent decrease of Al substitution, caused an increase in the unit-cell volume. This change was accompanied by an increase in the various metal$-$metal ($M-M$) distances.

Manceau *et al.* (2000) studied the local coordination environment of Cr, Co, Cu, Ni, Mn, and Zn in a natural goethite sample by EXAFS spectroscopy. Those authors observed that Cr, Ni, Cu, and Zn were preferably incorporated into the goethite structure, whereas Co and Mn were present in a hexagonal phyllomanganate impurity. Chromium, Cu, and Zn tended to adopt the same coordination symmetry both in natural and synthetic goethites. The authors observed no significant steric effects around Cu^{2+} and Zn^{2+} despite the 14% increase in ionic radii compared to Fe^{3+}. The Ni^{2+} site in synthetic goethite was strongly relaxed with a contraction of the goethite structure in the plane of edge-sharing double chains and an expansion in the direction of corner

linkages. They observed that this anisotropic relaxation of the Ni site locally reduced the distortion of the goethite crystalline structure, and this effect could be due to a clustering of Ni atoms.

Chromium, Zn, Cd, and Pb are environmentally important elements and, due to their co-occurrence with Fe in natural and anthropogenic environments (Wedepohl, 1969), tend to co-precipitate with Fe to form isomorphically substituted goethite. A comprehensive understanding of multi-metal incorporations in goethite is required because the nature and extent of metal associations vary from single-metal systems and this may be related to atomic structural changes taking place at a local scale (<4 Å). The incorporation of a certain metal may be limited or enhanced by the presence of the other metals and this knowledge is useful in environmental remediation and industrial processes to enhance or suppress incorporation of ancillary metals in goethite. The present investigation, therefore, focused on the multiple (di-, tri-, and tetra-) metal incorporations of Cr, Zn, Cd, and Pb in the goethite crystallographic structure. The structural parameters of metal-substituted goethites were investigated using synchrotron X-ray diffraction (SXRD) and X-ray absorption fine structure spectroscopy (XAFS), to gain an understanding of the changes that occurred in these parameters by varying the amount of metals incorporated, along with any synergistic and antagonistic effects of the co-metals.

MATERIALS AND METHODS

Sample preparation

Single-, two-, three-, and four-fold substituted goethites were prepared by mixing 62.5 mL of 0.9 M

$Fe(NO_3)_3$ solution with 62.5 mL of *xM* metal-nitrate solution(s) in 1 L, high-density polyethylene containers using a magnetic stirrer for 3 min. Throughout the study, *x* was 0.1 for single-, 0.05 for di-, 0.033 for tri-, and 0.025 for tetra-metal substituted goethites. A list of nominal (initial) concentrations used for the metals studied, Cr, Zn, Cd, and Pb, is given in Table 1. The overall nominal concentration was kept to 10 mole % in order to obtain maximum metal substitution and simultaneously avoid the formation of hematite and any spinel phase (Cornell, 1988). The mixtures of ferric and metal nitrate solutions were diluted to 375 mL with ultra-pure water (18 mΩ cm); 150 mL of 5 M KOH was added rapidly and the solution was stirred for ~2 min. The precipitates were further diluted to 1 L with ultrapure water. The initial pH of the suspensions was 13. The precipitates were aged at 70ºC for 40 days with intermittent shaking. The gas exchange was facilitated by opening the container lids for ~2 min every day. After aging, the clear supernatant was discarded. The precipitates were centrifuged and washed repeatedly with ultra-pure water to remove soluble salts and finally washed with acetone before drying at 40ºC. The solids were ground and checked for mineralogical purity using powder XRD (GBC MMA: CoKα radiation, λ = 1.7890 Å, operating conditions of 35 kV and 28.5 mA). Data were collected from 10−80º2θ using a step size of 0.02º2θ and a scan speed of 1.0º2θ min^{-1}.

X-ray amorphous and poorly crystalline materials were removed using 0.2 M oxalic acid/ammonium oxalate buffer (pH 3.0), in the dark, at room temperature for 2 h using a solid:solution ratio of 1:100. This process was repeated four times and the samples were finally washed with ultrapure water. The single-metal 'Pb'- containing samples were similarly washed with 0.2 M $HClO_4$, instead of oxalic acid/ammonium oxalate buffer, to avoid the formation of insoluble lead oxalate. Cadmium-substituted samples, showing $Cd(OH)_2$ peaks, were washed up to five additional times with 0.1 M $HClO_4$ to remove this impurity. The resulting, purified, crystalline samples were dried at 40ºC, ground gently, sieved through a 200 μm sieve, and rechecked for mineralogical purity using powder XRD.

Substitution analysis

Metal substitution in the purified goethite samples was determined by dissolving 10 mg of solid in 10 mL of 6 M HCl. The metal concentrations (Cr, Zn, Cd, Pb, and Fe) in the resulting solutions were measured using a Varian Vista AX inductively coupled plasma-atomic emission spectrophotometer.

Synchrotron XRD data collection and refinement

Synchrotron X-ray powder diffraction data were collected at beamline 20B of the Australian National Beamline Facility, at the Photon Factory (National Laboratory for High Energy Physics) in Tsukuba, Japan. The data were collected using X-rays of wavelength 0.9574 Å over the 5−45º2θ range and converted to digital format using a scanning step of 0.01º2θ. The data were analyzed by the Rietveld method (Rietveld, 1969) using Newton-Raphson strategy in *Rietica* 1.7.7 (Hunter, 1997). A pseudo-Voigt function was used to model the observed peak profiles. The initial unit-cell parameters and atomic coordinates were based on the *Pnma* space group of goethite (Szytula *et al.*, 1968). In the metal-substituted goethite, metals were

Table 1. Nominal and actual composition of single- and multi-metal substituted goethites.

Sample	Nominal *M* (%)	Structural *M*[a] (%)				Total metal substitution (%)
		Cr	Zn	Cd	Pb	
C_pure goethite	−	−	−	−	−	−
1_Cr	10.00	11.4	−	−	−	11.4
2_Zn	10.00	−	11.3	−	−	11.3
3_Cd	10.00	−	−	4.3	−	4.3
4a_Pb	10.00	−	−	−	2.7	2.7
4b_Pb	2.00	−	−	−	1.0	1.0
5_CrZn	5.00 e[b]	2.5	3.9	−	−	6.4
6_CrCd	5.00 e	5.3	−	5.2	−	10.5
7_CrPb	5.00 e	6.1	−	−	2.8	8.9
8_ZnCd	5.00 e	−	3.9	1.0	−	4.9
9_ZnPb	5.00 e	−	3.7	−	0.9	4.6
10_CdPb	5.00 e	−	−	5.5	1.1	6.6
11_CrZnCd	3.33 e	3.1	3.2	2.4	−	8.7
12_CrZnPb	3.33 e	3.8	3.2	−	1.3	8.3
13_CrCdPb	3.33 e	3.0	−	3.6	1.1	7.7
14_ZnCdPb	3.33 e	−	3.0	2.3	0.3	5.6
15_CrZnCdPb	2.50 e	3.0	2.6	2.0	0.4	8.0

[a] Structural $M = M \times 100/(Fe + M)$ (concentration in moles obtained by total chemical analysis of purified samples)
[b] nominal level of each metal.

assumed to occupy the same atomic position as Fe and the total occupancy factor was based on the extent of metal substitutions as obtained from the total chemical analysis.

XAS data collection and analysis

Data Collection. The EXAFS spectra of the metal-substituted goethites were collected at the K-edges of Cr (5989 eV) and Zn (9659 eV), and at the L_{III}-edge of Pb (13035 eV), and in selected cases at the Fe K-edge (7112 eV). Three to six spectra were collected for most of the samples to improve the signal to noise ratio.

X-ray absorption measurements were performed at room temperature at the Australian National Beamline Facility at the Photon Factory. X-ray absorption spectra were collected for Fe in transmission mode and for Cr, Zn, and Pb in fluorescence mode using a Canberra 36 element Ge solid state detector. For Cr and Fe, ion chambers filled with N_2 and Ar were used, whereas for Zn and Pb, He was used as a fill gas in the ion chambers. A channel-cut Si(111) double crystal monochromator was detuned by 20−50% to reject the higher-order harmonics and calibrated with respective metal foils, except in the case of Pb energy calibration, where a Au foil was used. The EXAFS spectra were collected at K/L_{III} edges over three regions (−200 to −30; −30 to +50; +50 to +900 eV) relative to the K/L_{III} edge) with increasing number of energy steps in each region. The Pb XANES spectra were collected in the range 12835 to 13055 eV with an energy step of 0.5 eV and a set-up similar to EXAFS data collection. Lead compounds, PbO, PbO_2, $Pb(CO_3)_2$, $Pb(OH)_2$, and $Pb(OH)_2CO_3$ from Gräfe *et al.* (2007), were used as Pb L_{III} reference materials.

The EXAFS spectra of singly Cd-substituted goethite were collected at the Cd K-edge at beamline 20-BM of PNC-CAT at the Advanced Photon Source, Argonne National Laboratory, Illinois, USA (Gräfe *et al.*, 2008). The Cd EXAFS data could not be obtained for the multi-metal substituted goethite.

Data analysis. The EXAFS spectra were analyzed using *Average* (Ellis and Freeman, 1995) and *WinXAS* v.2.3 (Ressler, 1998). Energy calibration of samples was carried out against corresponding metal foils. The spectra were corrected for background absorption and normalized by fitting first- and second-degree polynomials to the pre- and post-edge regions. The normalized XANES spectra for Pb were obtained similarly. The EXAFS was extracted after converting to K-space by specifying the threshold energy, E_o, using the first inflection point. The EXAFS oscillations were extracted using a cubic spline function with 7 knots over K ranges of 2.05−11.70 Å^{-1} for Fe, 2.15−12.71 Å^{-1} for Cr, 1.60−10.60 Å^{-1} for Zn, and 1.00−7.60 Å^{-1} for Pb. The EXAFS spectra, $\chi(k)$, were k^3-weighted and filtered with a Bessel window function and a smoothing parameter

($\beta = 4$) in order to minimize the ripple effects in the resulting radial structure function (R space). Fitting was performed in R space using one/two $M-O$ scattering paths and three $M-M$ scattering paths. The R ranges (uncorrected for phase shift functions) were kept at 0.75−3.73 Å for Fe, 0.75−3.63 Å for Cr, 0.70−3.60 Å for Zn, and 0.2−4.00 Å for Pb. The amplitude reduction factor (S_0^2) was fixed at 0.85 for Fe, 0.93 for Cr, 0.96 for Zn, and 0.70 for Pb fits. The k ranges, R ranges, and S_0^2 were kept constant for a particular metal in order to compare changes in its local coordination environment in the presence of different co-metals. The theoretical scattering paths were calculated with the *FEFF* 7.02 code (Rehr *et al.*, 1991). An *ATOMS* file was written using a structural model provided by Gualtieri and Venturelli (1999), using substituent metal as a core metal (instead of Fe) and then changing the scattering metal atom to Fe in the corresponding generated *FEFF* file. For each fit, the phase-shift value (ΔE_0) of each scattering path was correlated to the same value. Coordination numbers and inter-atomic distances (R) were allowed to float freely, while the Debye-Waller parameter (σ^2) was either set free or correlated to the same value among $M-O$ shells and $M-M$ shells.

RESULTS AND DISCUSSION

Mineralogical and chemical analyses of the solids

The XRD patterns of all the purified samples showed the presence of goethite only (Figure 2). Reflections due to cadmium hydroxide (β-Cd(OH)$_2$) were observed in the pattern for unpurified Cd-substituted goethite, with 10 mole % nominal Cd, and Cd- and Zn-substituted goethite, with 5 mole % nominal concentrations for each metal. A negligible amount of (β-Cd(OH)$_2$) was also observed in the patterns for the Cd- and Pb-substituted goethite, with 5 mole % nominal concentrations for each metal. Gerth (1990) also obtained a small fraction of (β-Cd(OH)$_2$) and otavite (CdCO$_3$) in addition to Cd-substituted goethite, at >5 mole % nominal Cd levels. No peaks indicative of β-Cd(OH)$_2$ were observed in the samples when Cd was mixed with Cr at any of the concentrations used in this study.

With increasing total metal substitution, the 101 peak shifted to greater d spacings and its full width at half maximum (FWHM) increased (Figure 3). Shifts in the diffraction peaks of metal-substituted goethite indicate anisotropy in the lattice expansion/contraction due to different metal(s) substitution(s) in the mineral structure. Goethite with 2.7 mole % Pb substitution (sample 4a_Pb) showed narrower diffraction peaks than the 1.0 mole % Pb-substituted sample (sample 4b_Pb) (Figure 2). The sharper diffraction peaks indicate well developed goethite crystals, which does not support the notion of Pb being incorporated in the goethite structure. A transmission electron microscope (TEM) image (Figure 4) shows the presence of small round particles
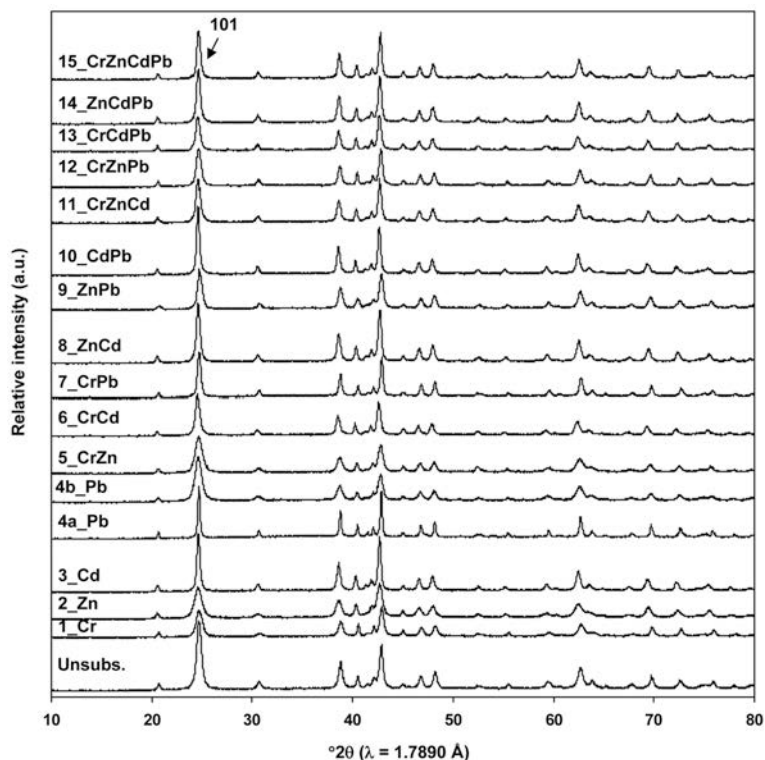
Figure 2. XRD patterns of pure and metal-substituted goethites after removal of X-ray amorphous and other impurities with ammonium oxalate and/or perchloric acid. The 101 diffraction peak for goethite indicated by the arrow shows displacement (°2θ) upon metal substitution.

adhering to the surfaces of well developed goethite crystals in this sample. These small particles were either X-ray amorphous or the goethite nuclei could not develop due to the substitution of much larger Pb^{2+} (1.19 Å) ions in the structure. The narrow diffraction peaks from goethite in this sample suggest the possibility that Pb incorporation was small in the well developed crystals and that the majority of Pb was associated with the small round particles.

In the single-metal systems, the extent of maximum metal incorporation in the goethite structure was Cr = Zn > Cd > Pb (Table 1). Similar levels have been reported in the literature; for example, Cr ≈ 10 mole % (Schwertmann *et al.*, 1989), Zn ≈ 9 mole % (Krehula *et al.*, 2006), Cd ≈ 6 mole % (Gerth, 1990), and Pb ≈ 2 mole % (Gerth, 1990). Huynh *et al.* (2003) reported greater incorporation of Cd, 9.5 mole %, in goethite without the formation of any other mineral. In contrast,
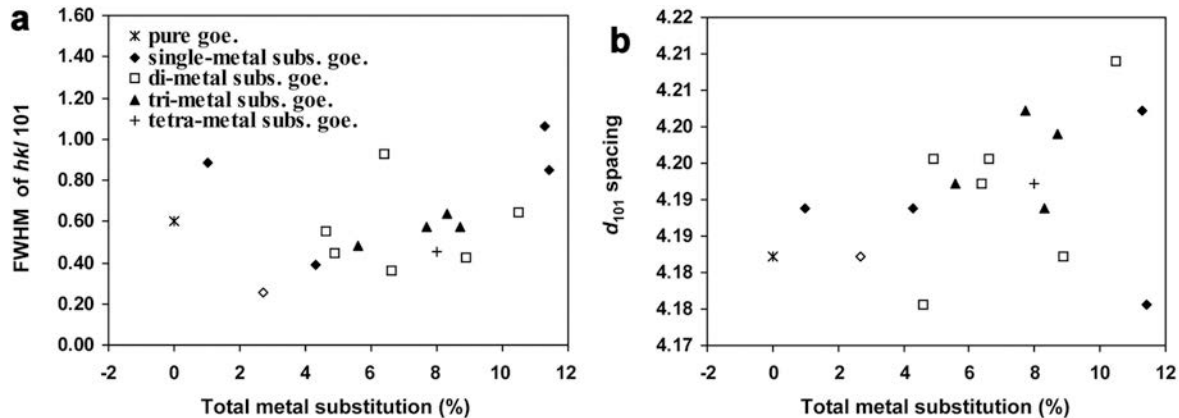

Figure 3. Changes in full width at half maxima (FWHM) (a), and *d* spacing (b) of the 101 diffraction peak with metal substitution in goethite. The open diamond indicates sample 4a_Pb.
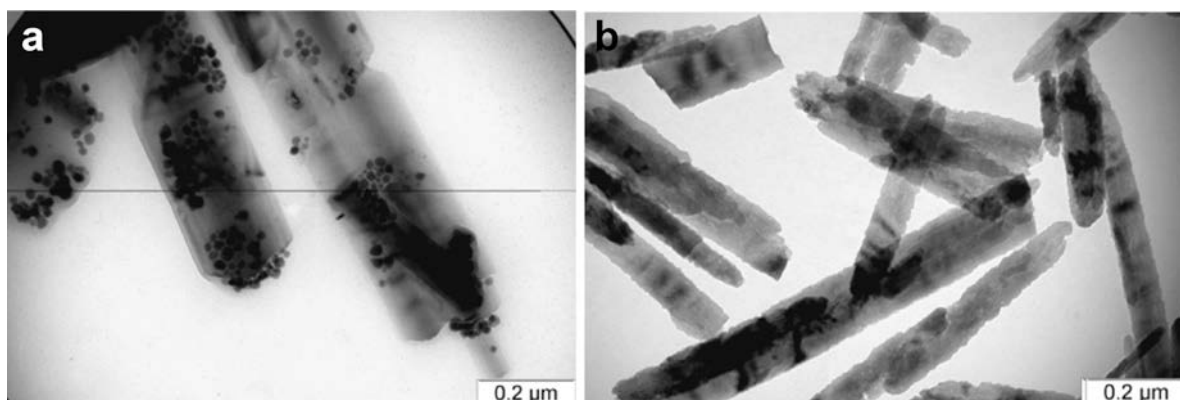
Figure 4. TEM images: (a) sample 4a_Pb showing small round particles adhering to the surfaces of well developed goethite crystals; (b) sample 7_CrPb showing the absence of nanoparticles.

Krehula and Music (2007) obtained goethite with Cd substitution of only 1.96 mole %; both goethite and hematite formed at Cd substitution of 2.91−6.98 mole % and hematite alone at Cd substitution of 9.09 mole %. The differences in Cd substitution levels in goethite could be attributed to differences in synthesis procedures. Huynh et al. (2003) synthesized Cd-incorporated goethites by precipitating the mixed solutions of 1 M $Fe(NO_3)_2$ and 1 M $Cd(NO_3)_2$ with 5 M KOH and aging the precipitates at 25ºC. Krehula and Music (2007) precipitated mixed solutions of $FeCl_3.6H_2O$ and $3CdSO_4.8H_2O$ with tetramethylammonium hydroxide and aged the precipitates at 160ºC. Krehula et al. (2006) obtained 11−13 mole % Zn incorporation in goethite, with <0.3 molar fractions of hematite and Zn-spinel ($ZnFe_2O_4$), under the same synthesis conditions as they used for preparation of Cd-substituted goethite.

In di-metal systems, Cr and Cd were incorporated in very large proportions, except in the presence of Zn (Table 1). The presence of Zn appeared to inhibit the incorporation of Cr and Cd. Conversely, incorporation of Cr and Cd was favored in the presence of each other, as well as in the presence of Pb (Table 1). The presence of

Zn had a substantial negative influence on the incorporation of Cd in the tri-metal system also (Table 1). One possible reason could be the formation of β-$Cd(OH)_2$ in the presence of Zn, in contrast to Pb and Cr, as is evident from the XRD analysis. The low solubility of β-$Cd(OH)_2$, K_{sp} (25ºC) $\approx 7.2 \times 10^{-15}$, as also suggested by the need for five additional washings with 0.1 M $HClO_4$ to remove this impurity from goethite, might decrease the amount of Cd^{2+} available for Fe^{3+} substitution in the goethite structure.

The incorporation of Zn was not affected by the presence of other metals in all multi-metal substituted goethites. The substitution of Fe^{3+} by Zn remained at ~4 mole % in di-metal and at ~3 mole % in tri-metal substituted goethites (Table 1). The incorporation of Pb was minimum (<2.8 mole %) among the studied metals in single- and multi-metal substituted goethite samples (Table 1). Previously, <2 mole % Pb incorporation was reported in goethite (Gerth, 1990; Ford et al., 1997; Martinez and McBride, 1998). Ford et al. (1997) and Martinez and McBride (1998) reported that a major proportion of Pb^{2+} was expelled from the crystalline phase during the transformation of ferrihydrite to
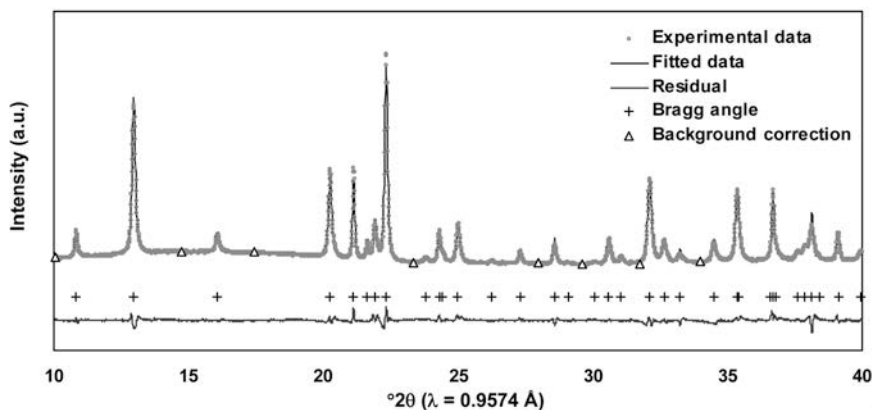

Figure 5. The Rietveld refinement of an SXRD pattern for a representative sample (10_CdPb sample).

goethite/hematite at 70ºC and pH 6. These authors speculated that Pb^{2+} substitution might occur in the initial amorphous material. However, after aging and thermal treatment at 70ºC, the solubility of Pb^{2+} in the goethite decreased because of the incompatibility of the ionic radius of Pb^{2+} (1.19 Å) with octahedral coordination. The presence of Cr (sample 7_CrPb) appeared to increase the incorporation of Pb in the bulk structure of goethite. Despite the similar level of Pb incorporation (2.8 mole %) to singly Pb-substituted goethite (sample 4a_Pb), no small round particles were observed in the TEM of the Pb,Cr-substituted goethite (Figure 4).

The range of total metal substitution became narrower as the number of metals increased in a given system (Table 1). For instance, the range was 1.0−11.4 mole % for single-, 4.6−10.5 mole % for di-, and 5.6−8.7 mole % for tri- and tetra-metal substituted goethites. In some cases, the incorporation of structural metal slightly exceeded the nominal metal concentration, *e.g.* in singly Cr- and Zn-substituted goethite, suggesting that the greater proportion of Fe, in comparison to *M*, was associated with the X-ray amorphous phase. In single-metal systems, a nearly linear relationship existed among ionic radii of substituent metals and their extent of substitution into the goethite structure ($R^2 = 0.87$). Conversely, no correlation was apparent between the extent of incorporation and ionic radii in the multiple metal systems.

Rietveld refinement of XRD data

The Rietveld refinements (see Figure 5 for a representative example, *i.e.* 10_CdPb) yielded acceptable fits to the observed diffraction data. The unit-cell parameters for pure goethite were within 99% accuracy of the ideal structure reported by Szytula *et al.* (1968) (Table 2). The *a*, *b*, and *c* unit-cell dimensions of goethite changed to the extents of 9.9346±0.1373, 3.0164±0.0362, and 4.6005±0.0504 Å, respectively, upon substitution of various metals (Table 2). The results showed deviations of up to 1.4% for *a*, 1.2% for *b*, and 1.1% for *c* unit-cell dimensions which imply that the sensitivity of the unit-cell parameters to disorder follows the order: $a > b > c$. Near linear relationships were observed between the various unit-cell dimensions and volume ($a{:}b$, $R^2 = 0.97$; $c{:}b$, $R^2 = 0.97$; $b{:}V$, $R^2 = 0.99$) (Figure 6).

The metal-metal ($M{-}M$) distances sharing O−OH edge (E_1) and OH−OH edge (E_2) changed by 3.0164±0.0362 and 3.3093±0.0414 Å, respectively (Figure 1, Table 2) and the double CS distance changed by 3.4332±0.0598 Å (Table 2). The percent deviations experienced by $M{-}M$ distances were: E_1, 1.20; E_2, 1.25; and CS, 1.74%. In contrast to the linear relationships between *a*, *b*, and *c*, no linear relationships were observed between the various $M{-}M$ distances, *e.g.* E_1 and E_2 ($R^2 = 0.54$) and E_2 and CS ($R^2 = 0.15$). The only significant linear correlation was between E_1 and CS $M{-}M$ distances ($R^2 = 0.82$). This shows that changes

occurring at short range ordering in goethite are complex, and could not be estimated directly from the changes occurring at the unit-cell scale.

Effects of metal substitutions on the unit-cell parameters of goethite

In the single-metal substituted Fe^{3+} (ionic radius of 0.645 Å) octahedra, the incorporation of Cr^{3+} (0.615 Å) decreased the unit-cell parameters whereas Zn^{2+} (0.74 Å), Cd^{2+} (0.95 Å), Pb^{2+} (1.19 Å), and Pb^{4+} (0.775 Å) increased the unit-cell parameters (Figure 7). Comparable values of unit-cell parameters have been reported in the literature, *e.g.* for Cr (Schwertmann *et*
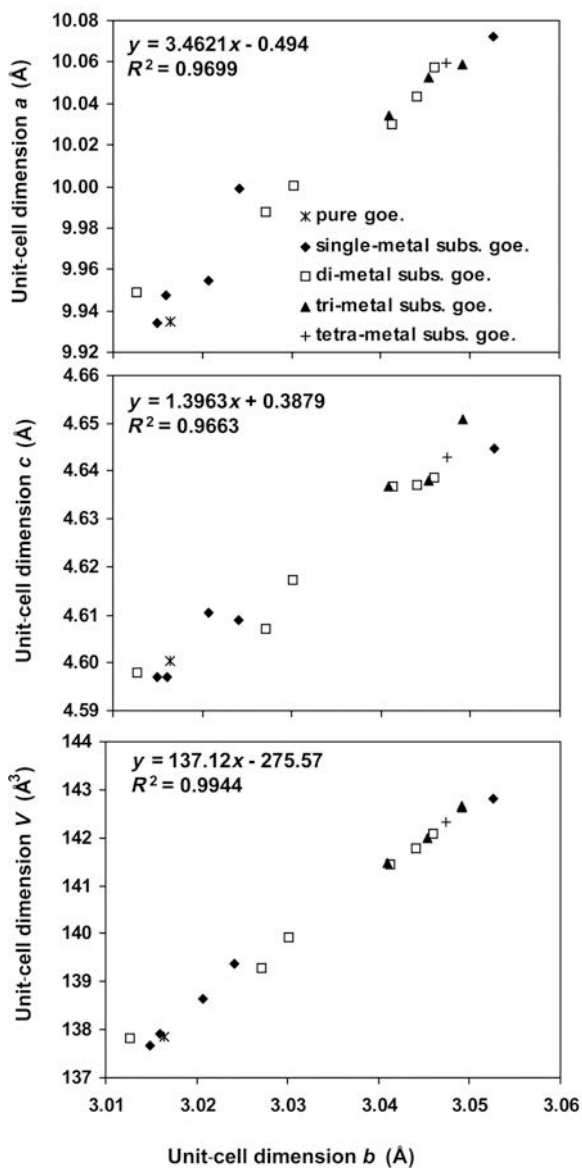

Figure 6. Linear relationships among unit-cell dimensions and unit-cell volume.

Table 2. Unit-cell parameters, $M-M$ distances and goodness of fit parameters for pure and metal(s)-substituted goethites as obtained from the Rietveld analysis.

Parameter	a (Å)	b (Å)	c (Å)	V (Å)³	E_1ᵇ (Å)	E_2ᶜ (Å)	CSᵈ (Å)	Rp (%)ᵍ	Rwp (%)	GOF (%)	R–Bragg
Cᵃ	9.9346 (4)ᵉ	3.0164 (1)	4.6005 (3)	137.86 (0.01)	3.0164 (1)	3.3093 (2)	3.4332 (1)	2.71	3.84	9.97	4.82
1_Cr	9.9340 (7)	3.0149 (3)	4.5970 (9)	137.68 (0.03)	3.0149 (3)	3.2957 (4)	3.4404 (5)	3.04	4.09	3.90	6.80
2_Zn	9.9986 (7)	3.0241 (2)	4.6090 (5)	139.36 (0.02)	3.0241 (2)	3.2885 (3)	3.4659 (3)	2.39	3.36	4.20	4.40
3_Cd	10.0719 (7)	3.0526 (2)	4.6446 (4)	142.80 (0.02)	3.0526 (2)	3.3399 (2)	3.4834 (2)	6.13	7.79	1.98	6.18
4a_Pb	9.9472 (2)	3.0160 (1)	4.5971 (1)	137.92 (0.01)	3.0160 (1)	3.3170 (1)	3.4330 (1)	3.04	4.09	3.90	6.80
4b_Pb	9.9545 (7)	3.0207 (2)	4.6105 (5)	138.64 (0.02)	3.0207 (2)	3.3070 (1)	3.4413 (2)	2.60	3.52	2.05	5.55
5_CrZn	10.0301 (9)	3.0413 (3)	4.6367 (9)	141.44 (0.04)	3.0413 (3)	3.3121 (4)	3.4824 (5)	6.36	8.19	2.31	6.43
6_CrCd	10.0002 (4)	3.0302 (1)	4.6171 (3)	139.91 (0.01)	3.0302 (1)	3.3111 (1)	3.4639 (1)	2.84	3.88	8.24	4.25
7_CrPb	9.9491 (2)	3.0127 (1)	4.5979 (2)	137.82 (0.01)	3.0127 (1)	3.2957 (1)	3.4458 (1)	2.18	3.16	5.69	4.42
8_ZnCd	10.0572 (8)	3.0460 (2)	4.6385 (6)	142.10 (0.02)	3.0460 (2)	3.3115 (2)	3.4930 (2)	6.40	8.38	1.01	6.55
9_ZnPb	10.0436 (9)	3.0441 (2)	4.6371 (6)	141.77 (0.03)	3.0441 (2)	3.3460 (3)	3.4648 (3)	7.17	9.03	0.03	7.54
10_CdPb	9.9877 (3)	3.0271 (1)	4.6071 (2)	139.29 (0.01)	3.0271 (1)	3.3252 (1)	3.4476 (1)	2.27	3.20	7.72	3.71
11_CrZnCd	10.0592 (8)	3.0491 (2)	4.6509 (6)	142.65 (0.02)	3.0491 (2)	3.3248 (3)	3.4917 (3)	6.64	8.62	1.75	7.66
12_CrZnPb	10.0340 (9)	3.0409 (2)	4.6367 (6)	141.48 (0.02)	3.0409 (2)	3.3296 (3)	3.4733 (2)	6.38	8.21	0.04	6.09
13_CrCdPb	10.0586 (9)	3.0491 (3)	4.6509 (8)	142.64 (0.03)	3.0491 (3)	3.3308 (3)	3.4869 (4)	9.09	11.7	1.49	7.83
14_ZnCdPb	10.0523 (6)	3.0453 (2)	4.6379 (5)	141.98 (0.02)	3.0453 (2)	3.3507 (2)	3.4654 (2)	6.18	7.89	1.62	7.41
15_CrZnCdPb	10.0595 (6)	3.0474 (1)	4.6428 (4)	142.33 (0.02)	3.0474 (1)	3.3302 (2)	3.4818 (2)	6.08	7.77	1.89	6.04

ᵃ C is pure goethite
ᵇ E_1 indicates distances between metal centers (Fe/M) of octahedra sharing an edge formed by O and OH
ᵈ E_2 indicates the distances between metal centers (Fe/M) of octahedra sharing an edge formed by two OH
ᵈ CS indicates distances between metal centers (Fe/M) of octahedra sharing a corner formed by one O
ᵉ The values in parentheses indicate error in the last digit.

al., 1989; Gerth, 1990; Sileo *et al.*, 2004), for Zn (Gerth, 1990), for Cd (Gerth, 1990; Huynh *et al.*, 2003), and for Pb (Gerth, 1990). The increase in the unit-cell volume for the 2.7 mole % Pb-containing sample (sample 4a_Pb) was negligible (0.04%) compared to 0.56% for the sample with 1 mole % Pb incorporation (sample 4b_Pb). This suggests that only a very small proportion of 2.7 mole % Pb in sample 4a_Pb was actually incorporated into the structure of goethite (Table 2), with the bulk of the Pb associating with the small, well rounded particles described above.

In the di-metal-substituted goethites, the expansion of the unit-cell parameters was maximum when the co-metal was Zn and was progressively smaller for co-metals Cd, Cr, and Pb, respectively (Figure 7).

Chromium and Cd caused smaller deviations in the unit-cell parameters (Figure 7) when present together or with Pb. This might be the reason for the synergistic effects of these metals on each other's structural incorporations in the di-metal-substituted goethite.

In the tri- and tetra-metal-substituted goethites, the individual effects of the substituent metals on the unit-cell dimensions were indistinguishable. Expansions in the unit-cell dimensions and unit-cell volumes of the tri- and tetra-metal-substituted goethites were essentially identical (Figure 7).

In samples containing Zn, the observed increase in the unit-cell parameters was insensitive to both the identity and the extent(s) of substitution of the co-metal(s) in the di-, tri-, and tetra-metal substituted
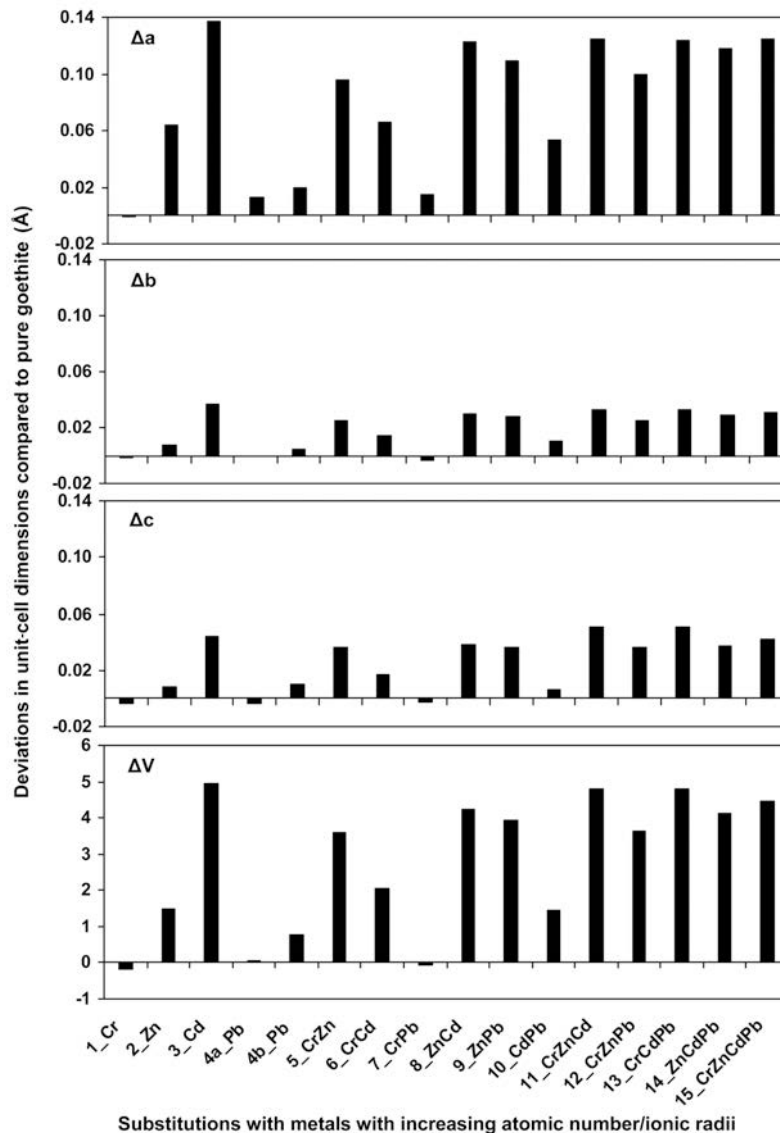

Figure 7. Changes in unit-cell dimensions (Δ*a*, Δ*b*, and Δ*c*) of goethite upon individual Cr, Zn, Cd, and Pb substitution, and in combinations of two, three, and all four metals.

goethites (Figure 7), illustrating, together with the similar levels of Zn substitution in the co-presence of Cr, Cd, and/or Pb, the dominant steric influence of structurally incorporated Zn.

In the single-metal substituted goethites, the unit-cell parameters and cell volume were linearly related to the ionic radii of substituent metals (R^2: $a = 0.82$ Å, $b = 0.88$ Å, $c = 0.95$ Å, and $V = 0.90$ Å^3). Gerth (1990) observed a linear relationship between the rate of change of b per unit of M substitution (Al^{3+}, Co^{3+}, Cr^{3+}, Mn^{3+}, Ni^{2+}, Cu^{2+}, Zn^{2+}, Pb^{4+}, and Cd^{2+}, Å/mole %) $vs.$ ionic radii of substituent metals in single-metal substituted goethites. No direct relationship between the unit-cell parameters (a, b, c, and V) and the extents of total metal incorporations in single- and multi-metal substituted goethites ($R^2 < 0.10$) was observed in the present work. The steric strains; a/b and a/c increased while c/b decreased upon incorporation of metal in the goethite structure (Figure 8). Among singly substituted goethites, the steric strains a/b and a/c followed the order Zn > Cd > Pb = Cr and c/b strains followed Cd > Zn = Pb > Cr (Figure 8). The large steric strains in Zn could partly explain its inhibiting effect on incorporation of other metals in goethite and the converse appears to be true for Cr.

The a:b and a:c strains were 0.08% and 0.22% greater, respectively, in the 4a_Pb goethite than in 4b_Pb goethite, contrary to smaller unit-cell V in the 4a_Pb goethite (Figure 8). Greater steric strains in sample 4a_Pb could explain the incorporation of less Pb in this compared to 4b_Pb. The steric strains among tri-metal-substituted goethites were similar (Figure 8), which may affect their narrow range of total metal substitution (Table 1). The steric strain in the multi-metal-substituted goethites lies within the steric strain ranges experienced by single-metal substituted goethites. For instance, in multi-metal-substituted goethites, the steric strains a:b and a:c were less than those observed in singly Zn-substituted goethite and c:b was less than that observed in singly Cd-substituted goethite (Figure 8).

Local coordination environments of substituent metals in metal-substituted goethites

The k^3-weighted EXAFS signals for Fe, Cr, Zn, and Pb in single-metal substituted goethite were similar to those observed for the tetra-metal-substituted goethite (Figure 9), indicating the uniformity in local coordination environments of Fe, Cr, Zn, and Pb in the presence of different co-metals. The corresponding Fourier Transform (FT) modulus and imaginary part were, however, dissimilar (Figure 9). This reflects differences in their nearest O co-ordinations and next nearest $M-M$ distances.

Local coordination environment of Fe(III). Analysis of the Fe EXAFS signal from the pure goethite sample showed that the Fe octahedra were asymmetric, with three O atoms at 1.96 Å and another three at 2.11 Å (Table 3). The three sets of Fe–Fe distances, i.e. E_1, E_2,

and CS, were 3.05, 3.29, and 3.44 Å, respectively (Table 3). The Fe–O/Fe distances were nearly identical to the ideal structure data, with accuracy of >98% (Szytula *et al.*, 1968). These Fe–Fe distances also agreed very well with those obtained from the Rietveld refinements. This implies that the local coordination environment of Fe is very similar to the average structure deduced from the Rietveld analysis. The results also demonstrate comparable accuracies in atomic distances as determined by EXAFS and SXRD techniques.

The Fe–O and Fe–Fe distances decreased slightly upon incorporation of the larger Cd^{2+}, Pb^{2+}, and Zn^{2+} cations into the goethite structure. The contraction in the
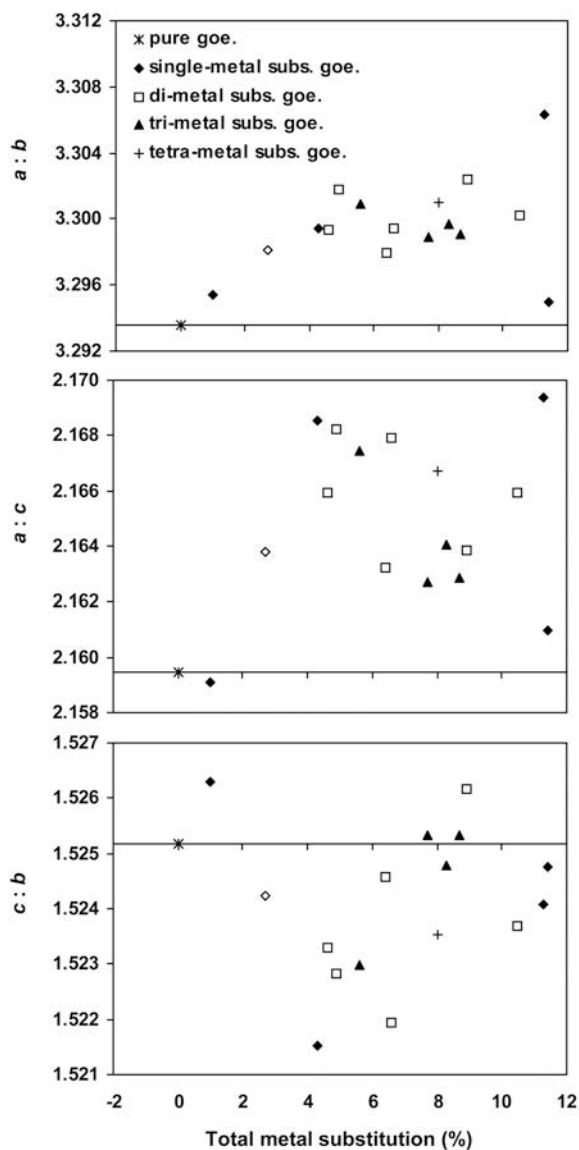

Figure 8. The plots of total metal substitution *vs.* steric strains; (a) a:b, (b) a:c, (c) c:b. The horizontal axis represents strains in pure goethite. The open diamond represents sample 4a_Pb.
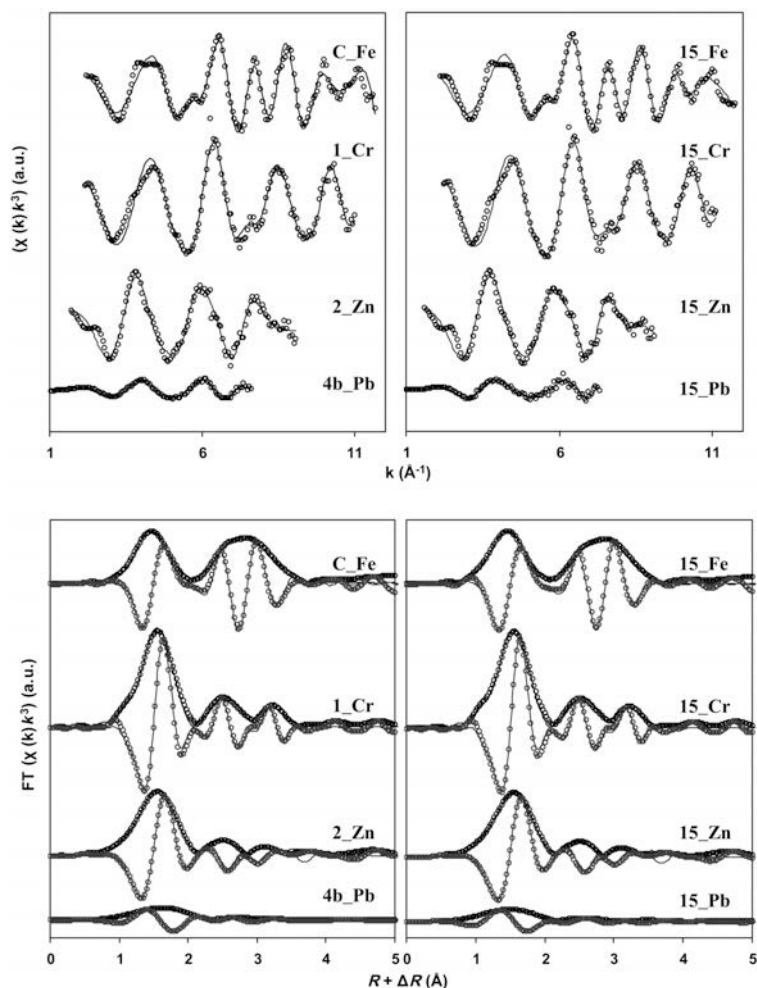
Figure 9. k^3-weighted Fe, Cr, and Zn K-edge and Pb L_{III}-edge XAFS spectra and corresponding modulus and the imaginary part of the Fourier transform of single- and tetra-metal substituted samples recorded at room temperature.

local Fe environment possibly occurred in order to accommodate the larger ions in the structure. The incorporation of Cr^{3+}, which has a smaller ionic radius than Fe^{3+} (0.645 *vs*. 0.615 Å), alleviated the contraction in the Fe local environment, *e.g.* sample 12_PbZnCr and 15_CdPbZnCr *vs*. sample 10_CdPb (Table 3). Sileo *et al*. (2004) also observed an increase in the Fe−M distance 'representative of E_2 and CS distances' from 3.37 to 3.40 Å with 12 mole % Cr substitution. Singh *et al*. (2002) observed the variations in the Fe−O distances from 1.92−2.01 and 1.96−2.31 Å and in the Fe−Fe distances from 3.00−3.05, 3.13−3.36, and 3.39−3.44 Å for single Cr-, Mn-, and Ni-substituted goethites, synthesized using $Fe^{(III)}$ procedures. The authors did not, however, observe any systematic changes in the Fe−O/Fe distances with the amount and type of element substituting in goethite. In contrast to these studies, Alvarez *et al*. (2007) observed that the various Fe−O and Fe−Fe distances remained practically constant upon simultaneous incorporation of Mn^{3+} and Al^{3+}.

Local coordination environment of Cr (III). In single-metal substituted goethite, the EXAFS analysis suggested that the Cr polyhedra were symmetric, *i.e.* all six O atoms were at the same distance (1.99 Å) from the central Cr atom (Table 4). The Cr polyhedra were smaller than Fe polyhedra with a Cr−O distance of 1.99 Å compared to an average Fe−O distance of 2.03 Å. Similar Cr polyhedra were observed in previous studies of Cr-substituted goethites (Singh *et al*., 2002; Sileo *et al*., 2004). The Cr−M distance, E_2, decreased substantially (3.22 Å) whereas the E_1 and CS distances were similar to the corresponding distances in pure goethite.

The local coordination environment of Cr remained practically the same as that observed in the single Cr-substituted goethite (Table 4) upon addition of the other cations (Zn, Cd, and Pb). In contrast to Fe, no effect of the co-substituting metal, *i.e.* Zn, Cd, or Pb, on the local co-ordination environment of Cr was observed. However, as seen before, the co-presence of Cr in Cd-,

Table 3. Structural parameters derived from the Fe K-edge EXAFS data of pure and selective multi-metal substituted goethites. The K range, R range, and S_0^2 were $2.05-11.7$ Å^{-1}, $0.75-3.73$ Å, and 0.85, respectively.

Sample	$R_{\text{Fe}-\text{O}}$[a] $(N_{\text{Fe}-\text{O}})$[b] $[\sigma^2]$[c] (1)	(2)	$R_{\text{Fe}-M}$ $(N_{\text{Fe}-M})$ $[\sigma^2]$			ΔE_0[d]	Residual
			E_1	E_2	CS		
C_Pure Goe.	1.96 (3.32) [0.005]	2.11 (2.61) [0.01]	3.05 (4.32) [0.01]	3.29 (2.98) [0.001]	3.44 (2.76) [0.001]	−1.60	5.88
10_CdPb	1.89 (1.08) [0.001]	2.03 (3.64) [0.007]	3.02 (2.29) [0.005]	3.25 (3.00) [0.006]	3.41 (3.12) [0.004]	−4.04	7.13
12_PbZnCr	1.94 (1.73) [0.004]	2.04 (3.16) [0.004]	3.03 (2.81) [0.005]	3.27 (2.01) [0.001]	3.42 (2.64) [0.002]	−3.87	7.77
14_CdPbZn	1.90 (2.41) [0.002]	2.04 (2.85) [0.003]	3.03 (3.00) [0.008]	3.26 (2.58) [0.002]	3.42 (3.36) [0.001]	−5.14	7.43
15_CdPbZnCr	1.93 (2.21) [0.003]	2.07 (3.04) [0.007]	3.05 (3.85) [0.01]	3.28 (2.52) [0.002]	3.43 (3.75) [0.002]	−3.37	6.52

[a] shell radius, estimated uncertainty ±0.03 Å
[b] coordination number, estimated uncertainty ±30% for O shell and ±50% for M shell
[c] Debye-Waller factor (Å^2)
[d] phase shift (eV)

Pb-, and Zn-substituted goethites reduced the contraction of Fe polyhedra. This may be a consequence of the smaller Cr polyhedra providing additional space to accommodate larger cations in the structure. These results suggest that Cr helps to alleviate the steric strains in the goethite structure induced by the addition of the larger cations (Zn, Cd, Pb).

Manceau *et al.* (2000) reported that Cr, Cu, and Zn had the same local structure in natural and synthetic goethite samples and that the presence of Mn, Co, Ni,

Table 4. Structural parameters derived from the Cr K-edge EXAFS data for single- and multi-metal substituted goethites. The K range, R range, and S_0^2 were $2.15-12.71$ Å^{-1}, $0.75-3.63$ Å, and 0.93, respectively.

Sample	$R_{\text{Cr}-\text{O}}$[a] $(N_{\text{Cr}-\text{O}})$[b] (1)	$R_{\text{Cr}-M}$ $(N_{\text{Cr}-M})$			σ^2[c]		ΔE_0[d]	Residual
		E_1	E_2	CS	Cr−O/Me	Cr−M (CS)		
1_Cr	1.99 (5.22)	3.02 (2.23)	3.22 (2.49)	3.45 (3.91)	0.005	0.009	−1.04	8.16
5_CrZn	1.99 (5.58)	3.02 (2.26)	3.22 (2.63)	3.45 (3.69)	0.005	0.009	−1.14	9.27
6_CrCd	1.99 (5.11)	3.03 (1.73)	3.24 (2.29)	3.46 (3.96)	0.004	0.009	−0.88	8.83
7_CrPb	1.99 (5.10)	3.02 (1.81)	3.24 (2.16)	3.46 (2.94)	0.003	0.005	−1.91	9.57
11_CrZnCd	1.99 (5.03)	3.04 (1.65)	3.26 (2.21)	3.48 (2.50)	0.001	0.002	−0.81	7.24
12_CrZnPb	1.99 (5.21)	3.02 (2.07)	3.22 (2.48)	3.45 (3.81)	0.004	0.009	−1.08	7.67
13_CrCdPb	1.99 5.70)	3.03 (2.15)	3.23 (2.63)	3.46 (4.30)	0.005	0.009	−1.29	8.81
15_CrZnCdPb	1.99 (5.45)	3.03 (1.89)	3.23 (2.29)	3.45 (3.54)	0.004	0.009	−1.02	7.88

[a] shell radius, estimated uncertainty ±0.03 Å
[b] coordination number, estimated uncertainty ±30% for O shell and ±50% for M shell
[c] Debye-Waller factor (Å^2)
[d] phase shift (eV)
[e] for Cr−O, Cr−M (E_1 and E_2).

Table 5. Structural parameters derived from the Cd K-edge EXAFS data in single-metal substituted goethite. The K range, R range, and S_0^2 were $1.00-10.45$ Å^{-1}, $1-4.00$ Å, and 0.71, respectively.

Sample	R_{Cd-O}[a] (N_{Cd-O})[b] (1)	R_{Cd-M} (N_{Cr-M}) E$_1$	E$_2$	CS	σ^2[c] Cd−O	Cd−M	ΔE_0[d]	Residual
3_Cd	2.21 (5.88)	3.15 (1.29)	3.33 (3.00)	3.54 (1.4)	0.003	0.005	−0.66	13.9

[a] shell radius, estimated uncertainty ±0.03 Å
[b] coordination number, estimated uncertainty ±30% for O shell and ±50% for M shell
[c] Debye-Waller factor (Å^2)
[d] phase shift (eV)

Cu, and Zn did not alter the Cr local coordination in natural goethite. The authors observed similar Cr−M distances as in the present study.

Local coordination environments of Cd(II). Similar to Cr, the Cd octahedra in singly Cd-substituted goethite were symmetric. The Cd−O distances (2.21 Å) were larger than the Cr−O distances (1.99 Å), however (Table 5). The expansion of the O shell around Cd atoms caused appreciable expansion of the E$_1$ and CS $M-M$ distances (Table 5). The increase in the $M-O$ distances around Cd^{2+} is consistent with its larger ionic radius (0.95 Å) as compared to Fe^{3+} (0.645 Å). These results are consistent with the increase in unit-cell parameters observed in the XRD analysis that could be attributed to expansion of the local coordination environment of Cd^{2+} in the goethite structure (Table 2).

Local coordination environments of Zn(II). The Zn polyhedra in the singly Zn-substituted goethite were asymmetric and more distorted than the Fe polyhedra in pure goethite. Four O atoms, in the equatorial plane, are at 2.08 Å and two O atoms in the axial distance at 1.93 and 2.24 Å (Table 6). This arrangement of O ligands did not alter the E$_1$ and E$_2$ distances significantly though it did enlarge the CS distance to 3.86 Å. This enlargement of the CS distances would disrupt the H-bonding located at empty double chains (Figure 1). This implies that Zn incorporation opens the goethite lattice. The configuration of ligands around the Zn^{2+} cation might occur to balance the local charge. The Zn octahedra were possibly Zn(OH)$_4$O$_2$, where 4OH$^-$ arranged themselves in equatorial positions, pushing one of the two O atoms further away axially which probably enlarged the CS distance. A similar local environment was observed for

Table 6. Structural parameters derived from the Zn K-edge EXAFS data in multi-metal substituted goethite. The K range, R range, and S_0^2 were $1.6-10.6$ Å^{-1}, $0.70-3.60$ Å, and 0.96, respectively.

Sample	R_{Zn-O}[a] (N_{Zn-M})[b] (1)	(2)	(3)	R_{Zn-M} (N_{Zn-M}) E$_1$	E$_2$	CS	σ^2[c] Zn−O	Zn−M	ΔE_0[d]	Residual
2_Zn	1.93 (1.43)	2.08 (3.74)	2.24 (1.37)	3.03 (2.33)	3.26 (3.54)	3.86 (1.86)	0.001	0.012	2.47	6.02
5_ZnCr	1.87 (0.50)	2.04 (4.37)	2.20 (1.61)	3.07 (3.55)	3.25 (3.12)	3.83 (1.89)	0.006	0.012	1.09	7.12
8_ZnCd	1.94 (1.91)	2.09 (3.76)	2.29 (1.05)	3.01 (2.79)	3.25 (2.74)	3.84 (1.31)	0.001	0.010	2.14	7.00
9_ZnPb	1.92 (1.32)	2.06 (3.82)	2.23 (1.47)	3.02 (3.67)	3.27 (3.51)	3.85 (1.32)	0.002	0.012	1.94	6.57
11_ZnCrCd	1.96 (2.24)	2.12 (3.74)	2.32 (1.09)	3.04 (3.95)	3.29 (4.17)	3.89 (1.09)	0.001	0.012	3.57	7.74
12_ZnCrPb	1.95 (1.71)	2.10 (3.69)	2.27 (1.03)	3.03 (4.07)	3.28 (4.03)	3.89 (1.56)	0.001	0.012	3.06	6.15
14_ZnCdPb	1.95 (1.24)	2.05 (4.22)	2.21 (1.56)	3.01 (3.34)	3.25 (3.28)	3.84 (1.66)	0.006	0.012	1.30	9.05
15_ZnCrCdPb	1.93 (1.66)	2.08 (3.93)	2.26 (1.36)	3.02 (3.41)	3.27 (3.32)	3.86 (1.33)	0.001	0.012	2.12	7.46

[a] shell radius, estimated uncertainty ±0.03 Å
[b] coordination number, estimated uncertainty ±30% for O shell and ±50% for M shell
[c] Debye-Waller factor (Å^2)
[d] phase shift (eV)

Ni in Ni-substituted goethites by Carvalho-E-Silva *et al.* (2003). Those authors attributed this atomic arrangement to the possible occurrence of $NiO_2(OH)_4$ instead of $FeO_3(OH)_3$, as a charge-balancing mechanism. The same charge-balancing mechanism for Ni-substituted goethite was first proposed by Singh *et al.* (2002).

The presence of Cr, Cd, and Pb in multi-metal substituted Zn goethites had no significant effect on the $Zn^{2+}-O$ and $Zn^{2+}-M$ distances which changed by ±0.06 Å (Table 6). This showed that the local coordination of Zn was unaffected by the presence of Cr, Cd, and Pb in the structure, and may be one of the reasons for practically the same extent of Zn substitution in the goethite structure in di- and tri-metal systems (Table 1). The local coordination environment of Zn was highly distorted in all cases and this apparently inhibited the incorporation of the other co-metals. The expansion of the local coordination around Zn with its larger ionic radius (0.775 Å) might be responsible for the enlargement of the unit cell of Zn-substituted goethites evident in the XRD studies. Manceau *et al.* (2000) reported similarity in Zn coordination environments in synthetic and natural goethite, despite the incorporation of Cr, Mn, Co, Ni, and Cu in the structure of the natural goethite. In contrast to the present study, Manceau *et al.* (2000) observed that the Zn coordination environment was similar to that of Fe in pure goethite. This difference is thought to reflect the very small levels (<3 mole % nominal level in the synthetic sample and, 0.026% in the natural sample) of Zn present in their samples.

Local coordination environment of Pb. The XANES spectra were collected for all singly and multi-metal-substituted Pb goethites. The normalized spectra for the samples and reference compounds are shown in Figure 10. The absorption edge for all Pb-substituted samples (except 4b_Pb) appeared at 13035 eV, which coincided with Pb^{2+} as in PbO and indicated the incorporation of Pb^{2+} rather than Pb^{4+} in goethite. The Pb absorption edge for the 4b_Pb sample was 13060 eV, corresponding to the value of PbO_2 (13060 eV), which suggested the occurrence of Pb in its tetravalent oxidation state. Oxidation of Pb^{2+} to Pb^{4+} could be attributed to the greater exposure to air of sample 4b_Pb than the other samples. The differences in the XANES features of the Pb-substituted samples and the $Pb(CO_3)_2$ argues against the presence of any $(CO_3)^{2-}$ ligands in the structure.

The Rietveld analysis showed a larger unit-cell volume and lesser steric strains for sample 4b_Pb as compared to sample 4a_Pb. Combining the results from chemical analysis, XRD, and XANES analyses, Pb^{4+} apparently was preferred over Pb^{2+} in the goethite structure and only a small proportion of Pb^{2+} was present in the structure. Based on the linear relationship between the ionic radius of Pb^{4+} and changes in the unit-cell parameters of Pb-substituted goethites, Gerth (1990)

speculated that substitution of Pb into the goethite structure occurred as Pb^{4+}.

The quantitative EXAFS analysis of the singly and multi-metal substituted goethites showed that the Pb polyhedra were asymmetric with two sets of O atoms at 2.15 and 2.31 Å (Table 7). This arrangement of O ligands left the E_1 and E_2 distances unchanged but enlarged the CS distance from 3.48 to 3.62 Å (Table 7). The CS distance was 3.49 Å in the Pb^{4+}-containing sample 4b_Pb, in comparison to 3.62 Å in the Pb^{2+}-containing sample 4a_Pb. The CS distance in sample 4b_Pb, approximately the same as seen in unsubstituted goethite, could explain the smaller steric strains in this sample compared to sample 4a_Pb. The CS distances of 3.62 Å are not impossible in the goethite structure; distances of up to 3.89 Å in Zn-substituted samples have been observed by the current authors. The expansion of the Pb^{2+} local environment was not reflected in the unit-cell dimensions derived from the Rietveld analysis of SXRD data. A major proportion of Pb^{2+} possibly resides in the peripheral layers of goethite crystals and the unit-cell parameters derived from the bulk structural analysis do not reflect the changes in the local environment around Pb.
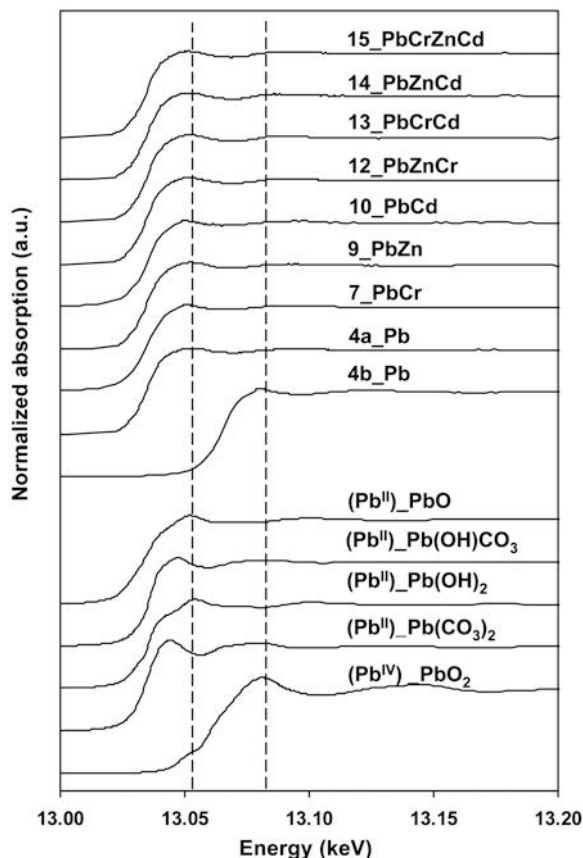

Figure 10. Pb L_{III} XANES spectra of Pb-substituted goethite and Pb reference compounds recorded at room temperature.

Table 7. Structural parameters derived from the Pb L_{III}-edge EXAFS data of multi-metal substituted goethites. The K range, R range, and S_0^2 were 1.0−7.6 Å^{-1}, 0.2−4.0 Å, and 0.7, respectively.

Sample	R_{Pb-O}[a] (N_{Pb-O})[b]		— R_{Pb-M} (N_{Pb-M}) —			σ^2[c]		ΔE_0[d]	Residual
	(1)	(2)	E_1	E_2	CS	Pb−O	Pb−Pb		
4a_Pb	2.15	2.31	3.01	3.27	3.62	0.002	0.009	−7.36	4.9
	(1.41)	(2.11)	(1.18)	(1.17)	(1.03)				
4b_Pb	2.19	2.29	3.09	3.27	3.49	0.005	0.007	−7.06	4.3
	(1.71)	(2.25)	(1.49)	(1.88)	(1.38)				
7_PbCr	2.15	2.31	3.05	3.26	3.48	0.002	0.004	−8.42	4.8
	(1.51)	(2.25)	(1.02)	(2.99)	(2.03)				
9_PbZn	2.16	2.36	3.11	3.30	3.54	0.001	0.001	−7.28	4.9
	(2.42)	(2.05)	(1.60)	(3.00)	(1.91)				
10_PbCd	2.13	2.29	2.97	3.26	3.62	0.001	0.010	−9.58	4.5
	(1.26)	(2.21)	(1.10)	(2.46)	(1.80)				
12_PbCrZn	2.15	2.36	3.08	3.28	3.52	0.003	0.005	−7.15	7.5
	(2.52)	(2.90)	(1.54)	(3.00)	(1.73)				
13_PbCrCd	2.18	2.31	3.09	3.32	3.61	0.003	0.007	−7.62	13.8
	(2.05)	(2.00)	(2.34)	(2.32)	(2.76)				
14_PbZnCd	2.20	2.43	3.19	3.34	3.57	0.006	0.007	−4.67	13.2
	(2.74)	(3.11)	(2.65)	(2.31)	(4.00)				
15_PbCrZnCd	2.15	2.35	3.06	3.29	3.53	0.001	0.001	−8.43	9.97
	(2.59)	(2.63)	(2.15)	(2.28)	(3.12)				

[a] shell radius, estimated uncertainty ±0.03 Å
[b] coordination number, estimated uncertainty ±30% for O shell and ±50% for M shell
[c] Debye-Waller factor (Å^2)
[d] phase shift (eV)

The coordination numbers of O and M atoms around Pb were ~25% less than the ideal ones (Table 7). This could be attributed to the low amplitude of the Pb-EXAFS signal (Figure 9) which possibly results from self absorption and/or the highly distorted coordination environment of Pb. The absence of Pb−M distances >3.62 Å eliminates the possibility of the presence of discrete Pb phases *i.e.* PbO, PbCO$_3$, Pb(OH)$_2$, and PbCO$_3$ (Gräfe *et al.*, 2007).

In Pb,Cr-substituted goethite, the Pb−M CS distance contracted to 3.48 Å, and the other Pb−M distances remained unaffected. This local environment of Pb was similar to that seen for the Fe in pure goethite, suggesting that the presence of Cr alleviated the distortion in the goethite structure due to Pb^{2+} incorporation. This tuning of the local distortion is correlated with the greater Pb^{2+} substitution (2.8 mole %) in the sample. Likewise, the presence of Al favors increased incorporation of Mn in Al,Mn-substituted goethite and the contraction of the Al octahedra, due to the smaller size of Al^{3+} compared to Fe^{3+}, reduced the axial distortion of the Mn cation, which in turn enhanced the extent of Mn incorporation into the goethite structure (Alvarez *et al.*, 2007).

The presence of Cd did not affect the Pb−O and Pb−M distances. It did, however, reduce the E_1 distance to 2.97 Å. On the contrary, the presence of Zn enlarged the Pb−M E_1, E_2, and CS distances to 3.13, 3.30, and 3.54 Å, respectively. The presence of Zn and, to some extent, Cd appeared to magnify the distortions in the local coordination of Pb. This could partly explain the synergistic effect of Cr and antagonistic effects of Zn and Cd on Pb incorporation in goethite. The antagonistic effect of Mn on Al incorporation in Al,Mn-substituted goethites was observed by Alvarez *et al.* (2007). The axial distortion of Mn limited the incorporation of Al in the structure.

In tri-metal systems, the Pb−M E_1 and E_2 distances increased to 3.19 and 3.34 Å, respectively. The distortions in local co-ordinations of Pb were greatest in the presence of Zn and Cd (Table 7). The presence of Cr in the tri- and tetra-metal substituted goethites moderated the increase in the Pb−O and Pb−M distances. For instance, in samples PbCrZn, PbCrCd, and PbCrZnCd, the two E_1 and E_2 distances fell within a narrow range of 3.08±0.02 and 3.30±0.02 Å, respectively. The extent of the distortions was greater in tri-metal substituted goethites than in di-metal substituted goethites. In a tetra-metal system, the greater number of co-metals appeared to limit the incorporation of Pb to very low levels (0.3 mole %) and consequently distortions of the structure tended to be very small.

The Rietveld and EXAFS analyses showed that, generally, the CS distance in the goethite structure was most affected by incorporation of an impurity cation. This could be attributed to the CS topology of the goethite structure. Structural analyses also showed that the substituent metals caused significant complex changes in the local coordination environments although the trends among unit-cell dimensions were linear. In

multi-metal systems, determination of the average structure is clearly insufficient to understand the complex changes occurring at the local scale. Moreover, the total metal substitution and changes on the unit-cell scale were not only influenced by ionic radii and charge-balancing mechanisms, but also by the presence of co-metal(s) in the system.

CONCLUSIONS

A significant amount (10 mole %) of simultaneous substitution of foreign cations can occur in goethite. Chromium and Cd have significant positive effects on their mutual incorporation and on the incorporation of Pb in the goethite structure. On the contrary, Zn limited the incorporation of Cr, Cd, and Pb in the structure of goethite. The results also imply that symmetric Cr/Cd octahedra reduce the overall steric strains in the structure compared to asymmetric Zn/Pb octahedra. Lead preferably resides as Pb^{4+} in the goethite structure. Critically, the present study demonstrates that the results from single-metal substituted goethite may not be applied to the natural environment where multiple elements may be associated with goethite.

REFERENCES

Alvarez, M., Rueda, E.H., and Sileo, E.E. (2007) Simultaneous incorporation of Mn and Al in the goethite structure. *Geochimica et Cosmochimia Acta*, **71**, 1009−1020.

Carvalho-E-Silva, M.L., Ramos, A.Y., Tolentino, H.C.N., Enzweiler, J., Netto, S.M., and Alves, M. (2003) Incorporation of Ni into natural goethite: An investigation by X-ray absorption spectroscopy. *American Mineralogist*, **88**, 876−882.

Cornell, R.M. (1988) The influence of some divalent cations on the transformation of ferrihydrite to more crystalline products. *Clay Minerals*, **23**, 329−332.

Cornell, R.M. (1991) Simultaneous incorporation of Mn, Ni and Co in the goethite (alpha-FeOOH) structure. *Clay Minerals*, **26**, 427−430.

Cornell, R.M. and Schwertmann, U. (2003) *The Iron Oxides: Structure, Properties, Reactions, Occurrences and Uses.*

Wiley-VCH Verlag Gmbh & Co. KGaA Weinheim, Germany.

Ellis, P.J. and Freeman, H.C. (1995) XFIT – an interactive EXAFS analysis program. *Journal of Synchrotron Radiation*, **2**, 190−195.

Ford, R.G., Bertsch, P.M., and Farley, K.J. (1997) Changes in transition and heavy metal partitioning during hydrous iron oxide aging. *Environmental Science & Technology*, **31**, 2028−2033.

Gerth, J. (1990) Unit cell dimensions of pure and trace metal-associated goethites. *Geochimica et Cosmochimia Acta*, **54**, 363−371.

Gräfe, M., Singh, B., and Balasubramaniam, M. (2007) Surface speciation of Cd(II) and Pb (II) on kaolinite by XAFS spectroscopy. *Journal of Colloid and Interface Science*, **315**, 21−32.

Gräfe, M., Mustafa, G., Singh, B., and Kookana, R.S. (2008) Solid phase partitioning of cadmium (Cd^{2+}) in goethite media. Pp. 187−204 in: *Adsorption of Metals by Geomedia II* (M. O. Barnett and D. B. Kent, editors). Developments in Earth and Environmental Sciences, **7**. Elsevier, Amsterdam.

Gualtieri, A. and Venturelli, P. (1999) In situ study of the goethite-hematite phase transformation by real time synchrotron powder diffraction. *American Mineralogist*, **84**, 895−204.

Hunter, B.A. (1997) *Rietica for Windows* v. 1.7.7. ANSTO, Sydney, Australia.

Huynh, T., Tong, A.R., Singh, B., and Kennedy, B.J. (2003) Cd-substituted goethites − A structural investigation by synchrotron X-ray diffraction. *Clays and Clay Minerals*, **51**, 397−402.

Krehula, S. and Music, S. (2007) The influence of Cd-dopent on the properties of alpha-FeOOH and alpha-Fe_2O_3 particles precipitated in highly alkaline media. *Journal of Alloys and Compounds*, **431**, 56−64.

Krehula, S., Music, S., Skoko, Z., and Popovic, S. (2006) The influence of Zn-dopant on the precipitation of alpha-FeOOH in highly alkaline media. *Journal of Alloys and Compounds*, **420**, 260−268.

Manceau, A. and Drits, V.A. (1993) Local-structure of ferrihydrite and feroxyhite by EXAFS spectroscopy. *Clay Minerals*, **28**, 165−184.

Manceau, A., Schlegel, M.L., Musso, M., Sole, V.A., Gauthier, C., Petit, P.E., and Trolard, F. (2000) Crystal chemistry of trace elements in natural and synthetic goethite. *Geochimica et Cosmochimica Acta*, **64**, 3643−3661.

Martinez, C.E. and McBride, M.B. (1998) Coprecipitates of Cd, Cu, Pb and Zn in iron oxides: Solid phase transformation and metal solubility after aging and thermal treatment. *Clays and Clay Minerals*, **46**, 537−545.

Rehr, J.J., Mustre de Leon, J., Zabinski, S.I., and Albers, R.C., 1991. (1991) Theoretical X-ray absorption fine structure standards. *Journal of the American Chemical Society*, **113**, 5135−5145.

Ressler, T. (1998) WinXAS: a program for X-ray absorption spectroscopy data analysis under MS-Windows. *Journal of Synchrotron Radiation*, **5**, 118−122.

Rietveld, H.M. (1969) A profile refinement method for nuclear and magnetic structures. *Journal of Applied Crystallography*, **2**, 65−71.

Schwertmann, U., Gasser, U., and Sticher, H. (1989) Chromium-for-iron substitution in synthetic goethites. *Geochimica et Cosmochimica Acta*, **53**, 1293−1297.

Sileo, E.E., Ramos, A.Y., Magaz, G.E., and Blesa, M.A. (2004) Long-range vs. short-range ordering in synthetic Cr-substituted goethites. *Geochimica et Cosmochimica Acta*, **68**, 3053−3063.

Singh, B. (2001) Heavy metals in soils: sources, chemical reactions and forms. Pp. 77−93 in: *Environmental*

Geotechnics (D. Smith, S. Fityus, and M. Allman, editors). Proceedings of the 2nd Australia and New Zealand Conference on Environmental Geotechnics − Geoenvironment 2001. Australian Geochemical Society, Newcastle, Australia.

Singh, B. and Gilkes, R.J. (1992) Properties and distribution of iron oxides and their association with minor elements in the soils of south-western Australia. *Journal of Soil Science*, **43**, 77−98.

Singh, B., Harris, P.L., and Wilson, M.J. (1997) Geochemistry of Acid Mine waters and the role of micro-organisms in such environments: a review. *Advances in Geoecology*, **30**, 159−192.

Singh, B., Sherman, D.M., Gilkes, R.J., Wells, M.A., and

Mosselmans, J.F.W. (2002) Incorporation of Cr, Mn and Ni into goethite (α-FeOOH): mechanism from extended X-ray absorption fine structure spectroscopy. *Clay Minerals*, **37**, 639−649.

Szytula, A., Burewicz, A., Dimitrijevic, Z., Krasnicki, S., Rzany, H., Todorovic, J., Wanic, A., and Wolski, W. (1968) Neutron diffraction studies of α-FeOOH. *Physica Status Solidi*, **26**, 429−434.

Wedepohl, K.H. (1969) *Handbook of Geochemistry*. Springer, Berlin, Heidelberg, New York.